ICONHIC 2016
1st International Conference on Natural Hazards & Infrastructure
28-30 June, 2016, Chania, Greece

Buried Pipeline subjected to normal fault offsets: the key role of soil dilatancy in pipeline design

A. Tsatsis[1], F. Gelagoti, G. Gazetas
National Technical University of Athens

ABSTRACT

Buried pipelines often cross tectonically active areas capable of producing large earthquakes and large ground deformations. Based on the observed damage mechanisms during past earthquakes, buried pipelines has shown a distinctive vulnerability to faulting-induced ground movements This study numerically investigates the response of an infinitely long pipeline subjected to normal fault. Emphasis is being placed on the effect of the dilative behavior of the soil. It has been long recognized that the dilative response of the soil may lead to an increase in the soil restrain to axial pipe movements. Namely, during axial pull-out a shear zone along the circumference of the pipe is formed. In case of a dilative soil, the shearing of this zone is accompanied by a tendency towards expansion. The constraint of this volumetric change results in increased normal stresses at the pipe-soil interface that in turn, provoke higher values of axial capacity. In order to rigorously assess the actual soil resistance to axial pipe movements, accounting for the effect of the soil dilatancy, a step-by-step numerical methodology is introduced. It is shown that when embedded in dilative soil, the maximum offset that a pipeline can attain before failure is substantially decreased (compared to the case of a non-dilative soil). Therefore, ignoring the tendency of soil towards may lead to an un-conservative design.

Keywords: pipe, 3D finite element modeling, dilative behavior

INTRODUCTION

Pipelines often pass through tectonically active areas and may cross active faults capable of producing large earthquakes and large ground deformations. There are various examples of past earthquakes that caused severe damage to buried pipelines, such as the earthquakes of Northridge 1994, Kobe 1995, Chi-Chi 1999, Kocaeli 1999 and more recently Chile 2010, Christchurch 2010-2011, and Japan 2011. Based on the observed failure mechanisms (e.g. O'Rourke and Palmer 1996, Uzarski end Arnold 2001, Tang 2000), buried pipelines has shown a distinctive vulnerability to permanent ground deformations associated with the seismic incidents rather than the transient ground displacements caused by the passage of seismic waves (Liang and Sun 2000). Although less frequent, permanent ground displacements impose large axial and bending strains that may lead to material rupture, either due to tension or due to buckling.

An example of such permanent ground displacement is the emergence of a normal fault to the ground surface. A fault is classified as normal when the relative slip takes place on the vertical direction and the moving block (hanging wall) moves downwards with respect to the stationary block (footwall). In the unfortunate case where such a fault intersects with a pipeline, it imposes an abrupt step-like deformation. As schematically presented in Figure 1, due to the inclined fault rupturing, the pipeline is subjected to both axial (δx) and vertical (δz) displacements. The vertical differential displacement is accommodated within a limited length at the vicinity of the fault trace, while the axial displacement affects a significantly larger pipeline length. Three regions can be recognized based on the type of stressing of the pipe: a central region at the vicinity of the fault trace

[1] Corresponding Author: A. Tsatsis, *National Technical University of Athens, ag_tsa@yahoo.gr*

(segment AB), where the pipe distress is three-dimensional (it is stressed axially due to the imposed stretching, it bends under the vertical differential displacement and deforms in the transversal direction due to the consequent hoop stresses), and two regions beyond the central segment (segments A'A and BB'), where the stressing of the pipe is one-dimensional (practically exclusively due to stretching).

Invariably, a potential pipe failure will take place within the central region (AB) where the stressing is adverse. The combination of large axial forces (that are getting larger at the vicinity of the imposed dislocation) with the bending moment are resulting in extreme strain demands which may ultimately cause rupture of the pipe wall. Inevitably, to account for this highly complicated 3D stressing conditions, the analysis of this pipeline segment (AB) should involve the accurate modeling of the inelastic material behavior of the pipe and the surrounding soil, as well as the accurate representation of the actual contact conditions between the soil and the pipe g .

On the other hand, of equal importance is the realistic modelling of the pipeline response beyond the central region AB. Since the pipeline is not fixed at the ends of segment AB, but extends far away, it introduces flexibility at the two boundaries that should be correctly captured. . The stiffer the axial response of the segments A'A and BB', the larger the tensile strains due to stretching will be. On the other hand, a more compliant response of the segments A'A and BB' will result in a relief in strain accumulation. Consequently, the accurate simulation of the axial response of the pipe segments (beyond the central critical region) may be the catalyst between the correct or false prediction of the entire pipeline response.

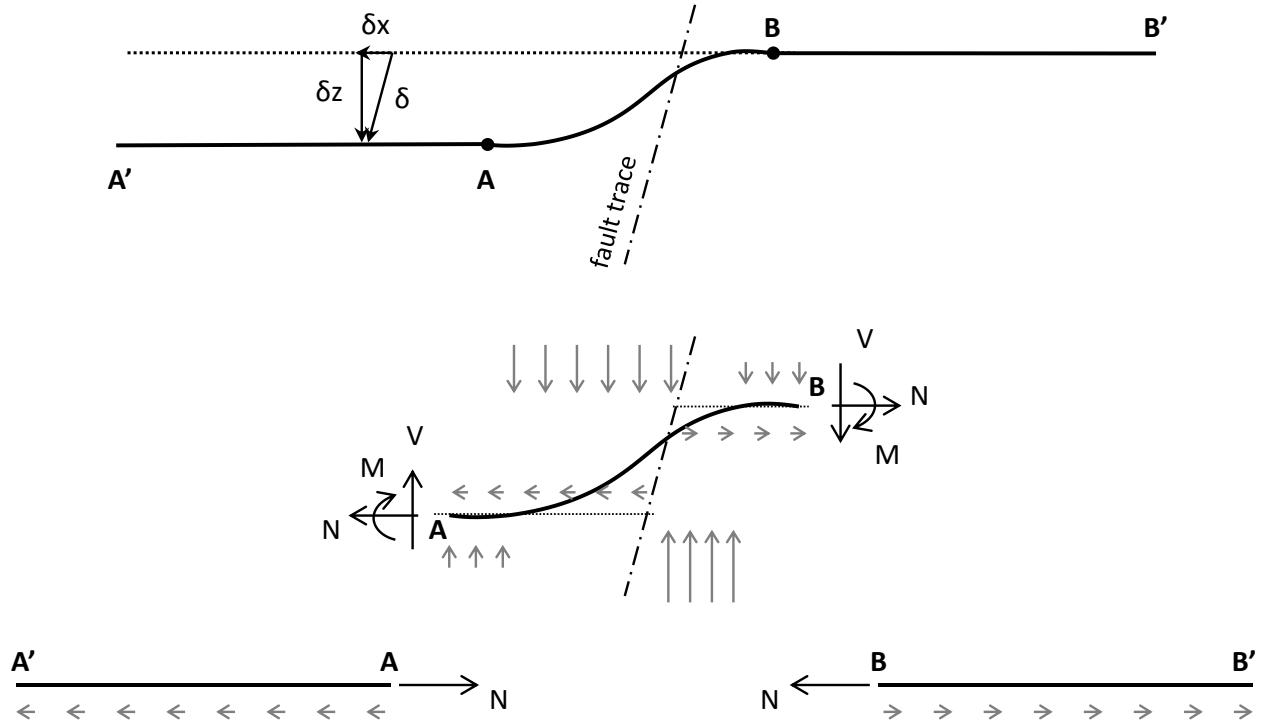

Figure 1. Infinitely long pipeline subjected to normal faulting. Three regions can be recognized based on the type of stressing: a central region at the vicinity of the fault trace where the pipe is stressed due to bending and stretching (segment AB), and two regions beyond the central segment where the stressing of the pipe is practically purely axial (segments A'A and BB').

Axial Pipeline Performance

Typically the Pull-Out Resistance of the Pipeline is determined by Eq. 1 (as described in the ALA 2001, and PRCI 2004 guidelines) :

$$T_{max} = \pi DH\gamma[(1+Ko)/2]\tan\delta \quad (1)$$

where D is the pipe outside diameter, H the depth to pipe centerline, γ the effective unit weight of the soil, Ko the coefficient of pressure at rest and δ the interface angle of friction between the pipe and the soil.

Yet, scarce experimental evidence on pull-out tests of buried pipelines. Singhal (1980), Colton, J. et al. (1982), Capalletto et al. (1998), Honegger (1999)] designate a rather interesting finding: the maximum axial load of pipes embedded in dense sands is significantly higher than that predicted by Eq1. In the same pace is the work of Paulin et al (1998), who have conducted full-scale axial pullout tests buried in sands and clays. =and the work of Anderson (2005) who conducted a series of pullout tests on straight and branched buried HDPE pipes in loose and dense sand. Recently, Wijewickreme et al (2009) measured the soil pressure during the pullout tests in dense sand and concluded that the overall normal soil stresses on the pipe during the pullout increased substantially compared to the initial (at rest) values. According to the authors, T=this increase was attributed to the constrained dilation along the pipe periphery during shear deformations.

Scope of this study is to investigate the effect of the dilative behavior of a dry sand on the performance of a buried steel pipeline subjected to normal faulting. The analysis of the mechanical behavior of the pipe is conducted using advanced numerical tools, accounting rigorously for the inelastic behavior of the pipe and the surrounding soil, the contact between the pipe and the soil (including sliding and gap formation), as well as any interaction phenomena between the two. Particular emphasis is given to the introduction of a step-by-step numerical methodology for the estimation of the actual soil resistance to relative longitudinal displacement of the pipe, accounting for the effect of the soil dilatancy.

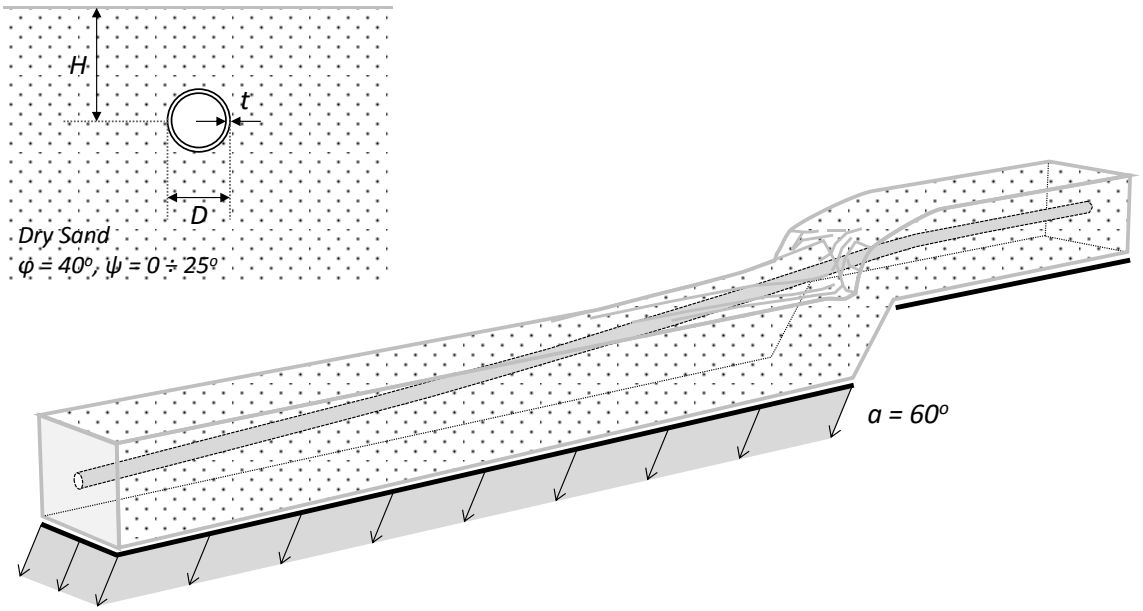

Figure 2. The studied problem: an infinitely long pipeline (D=36 in, t=12.7 mm, H=1.66 m), buried in dry sand (γ=17 kN/m^3, φ=40^o, ψ=0÷25^o] is subjected to normal fault (a=60^o).

PROBLEM DEFINITION AND ANALYSIS METHODOLOGY

The paper studies the structural performance of an infinitely long buried steel pipeline subjected to normal faulting (Figure 2). For the purposes of this study a rather typical hydrocarbon transportation pipeline is considered. The pipeline is assumed to be steel of grade X65 (σ_y = 450 MPa). It has been designed for maximum operating pressure p_{max} = 9 MPa. Assuming an outer diameter of D = 36 in, the required pipeline thickness is given by the Eq.2, and is equal to t = 12.7 mm = (The code of Federal Regulations of the U.S., 49 CFR 192.105):

$$p_{max} = 0.72*(2\sigma_y t/D) \quad (2)$$

To render the results more realistic the pipeline is considered to function under operating pressure p_{oper} = 6 MPa. It is embedded within the soil at depth 1.2 m from the surface to the pipe crown (H = 1.66 m).

The surrounding soil is a dry sand with unit weight $\gamma = 17$ kN/m^3, peak friction angle $\varphi = 40^o$ and residual friction angle $\varphi_{res} = 32^o$. The dilation angle ψ ranges parametrically between 0^o and 25^o. The fault trace is perpendicular to the pipeline axis and has a dip slip $a = 60^o$.

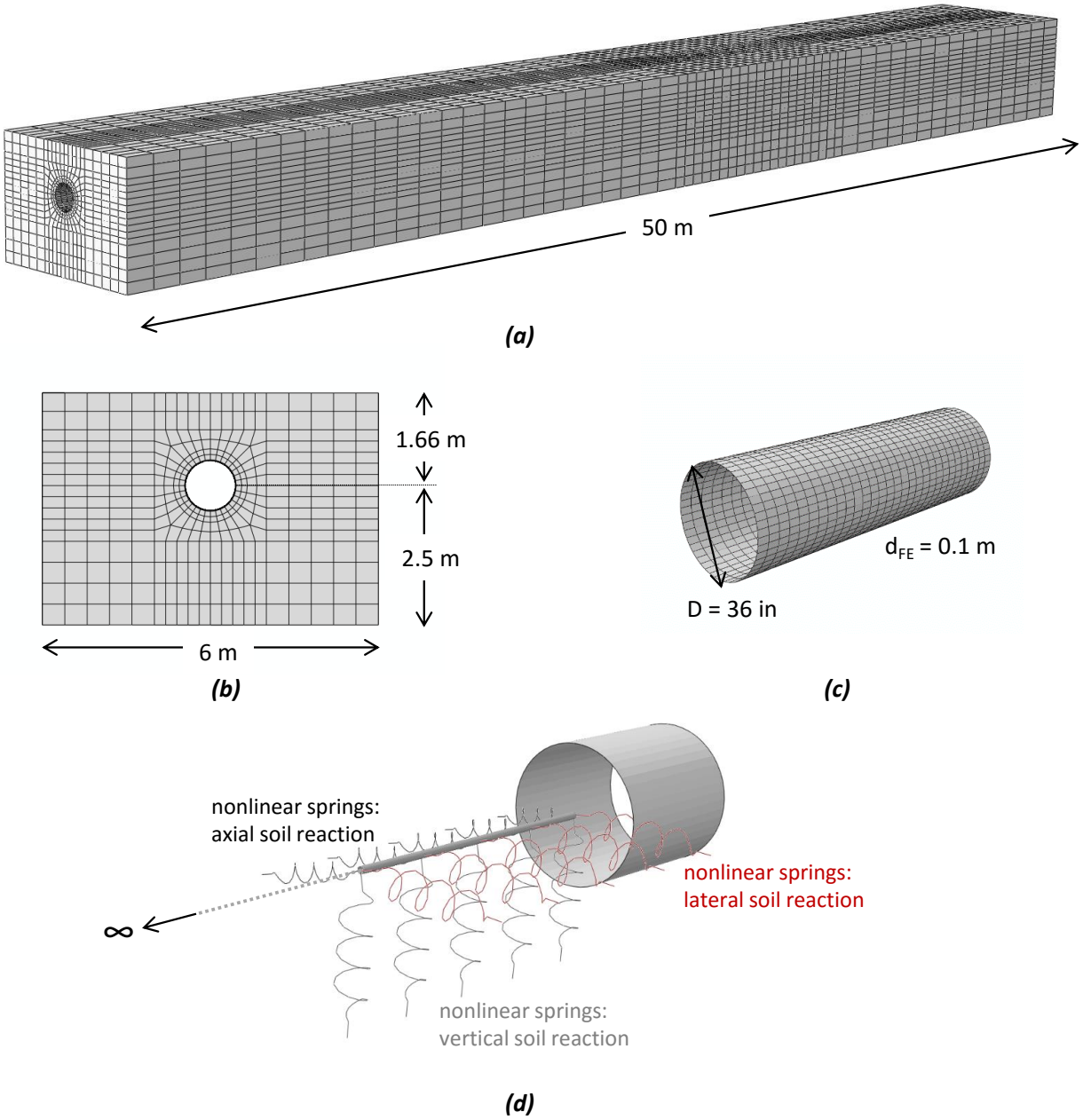

Figure 3. Details of the numerical model (a) The central region (at the vicinity of the rupture) is modeled with 3D FE. (b) a cross-section of the 3D model. (c) Shell elements for the pipe mesh. (d) Beyond the boundaries of the 3D model the pipe is represented by beam elements and the soil reactions with appropriate (independent) nonlinear springs in x,y,z directions.

The pipeline length that is affected by the slip along the fault trace is quite large. The simulation of that length in three dimensions would result in a finite element model with an excessively large number of elements, rendering such an analysis practically impossible at least with current computational power. To overcome this problem, the finite element model is divided in three parts that correspond to the three regions of distinctively different behavior that have been already discussed. At the vicinity of the fault the problem is analyzed in three dimensions to accurately simulate all the complex phenomena of the pipe and the soil response. A soil prism

of total length of 50 m along with the respective pipeline segment is considered. We assume that this limited length is adequate for the pipe to accommodate the vertical displacement due to faulting. Details of the finite element model employed in this study are presented in Figure 3. The soil is modeled with hexahedral (8-noded) brick-type elements of dimension d_{FE} = 0.25 m at the immediate vicinity of the rupture to allow proper modelling of the shear localization. The pipeline is modeled with 4-noded reduced-integration shell elements of longitudinal dimension d_{FE} = 0.1 m. The circumference of the pipe is discretized in 48 shell elements. An elastoplastic Mohr–Coulomb constitutive model with isotropic strain softening is employed to model nonlinear soil behavior (Anastasopoulos et al. 2007). Strain softening is introduced by reducing the mobilized friction angle φ_{mob} and the mobilized dilation angle ψ_{mob} with the increase of octahedral plastic shear strain.

As for the steel pipeline, elastic–perfectly plastic material behavior is considered, assuming σ_y = 450 MPa and E_{steel} = 200 GPa (corresponding to steel grade X65). To realistically simulate the interface between the pipeline and the soil, a special contact interface is introduced, allowing for realistic modeling of sliding of the pipeline relative to the surrounding soil (assuming Coulomb friction between the steel and the soil material), as well as soil detachment (i.e., not allowing tensile stresses to develop, leading to separation between the soil and the pipeline).

Outside from the central 3D mesh, the pipeline is practically stressed exclusively by the imposed stretching (one-dimensional response). As such, we have introduced a less complicated modeling where the pipe is represented by beam elements, and the soil reactions are modeled with nonlinear springs. The force-displacement behavior in each direction is calculated through finite element uniaxial push tests (++add Reference to your previous paper). Special care is placed in the correct calculation of the axial force-displacement response accounting for the effect of the dilation. Towards this direction a finite element based methodology is introduced and presented in the ensuing.

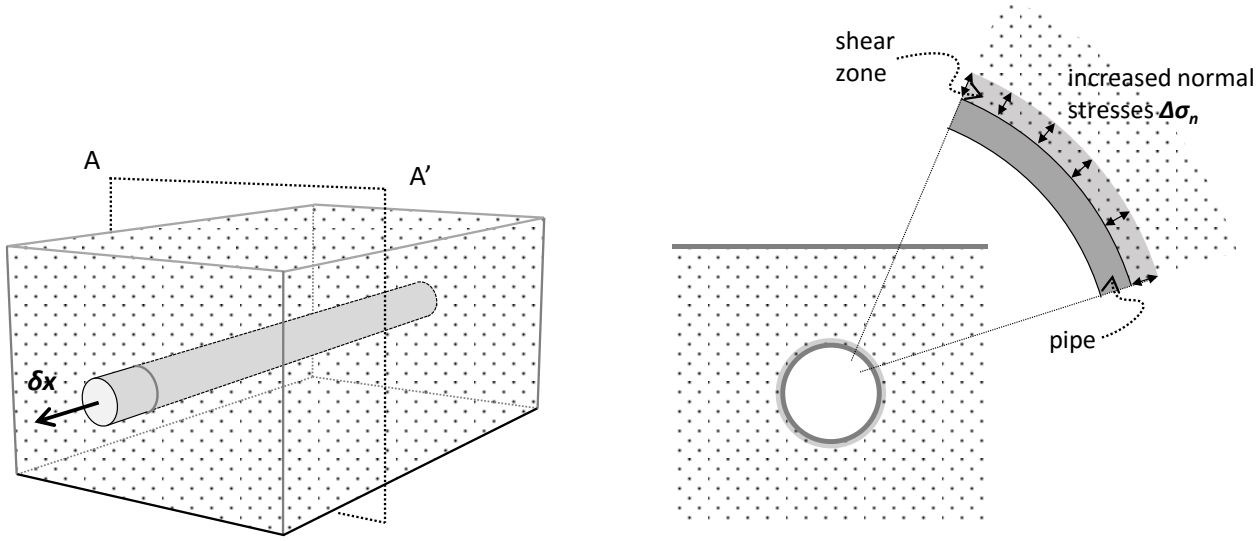

Figure 4. During axial movement of the pipe, the overall normal soil stresses on the pipe during pullout increased substantially in comparison with the initial values. This increase was attributed to the constrained dilation of the thin shear zone.

AXIAL SOIL RESTRAIN OF A DILATIVE SAND

As stated previously, several researchers have already observed the increase in the axial load on pipes during pullout tests when embedded in dilative soils. This increase was attributed to the constrained dilation during shear deformations (Figure 4). As the pipe is pulled in the longitudinal direction, the soil resists the movement through shearing that is concentrated in a thin zone around the pipe. Roscoe (1970) and Bridgewater (1980) suggested that the thickness of this shear zone (considered typical of an actively sheared zone in direct-shear mode of straining) is about 10 times the mean particle size d_{50}, while according to Vardoulakis and Graf (1985) its thickness is $16d_{50}$. Based on micro-scale particle image velocimetry (PIV) observations, DeJong et al. (2006) suggested that the thickness of this shear band approximately 5 - 7 particle diameters.

In cases of dilative soils, this shear zone tends to expand radially, an expansion that is confined by the pipe on the one side and the soil on the other side. As a result, during axial displacement of the pipe a parasitic stress $\Delta\sigma_n$ is developed that acts normal to the pipe. Therefore, the initial normal stresses on the pipe may increase significantly during the axial pullout test producing a proportionate increase of the maximum axial force. To account for these small-strain effects in conventional FE modeling a step-by-step numerical methodology is introduced, which may be described by the flowchart of Figure 5.

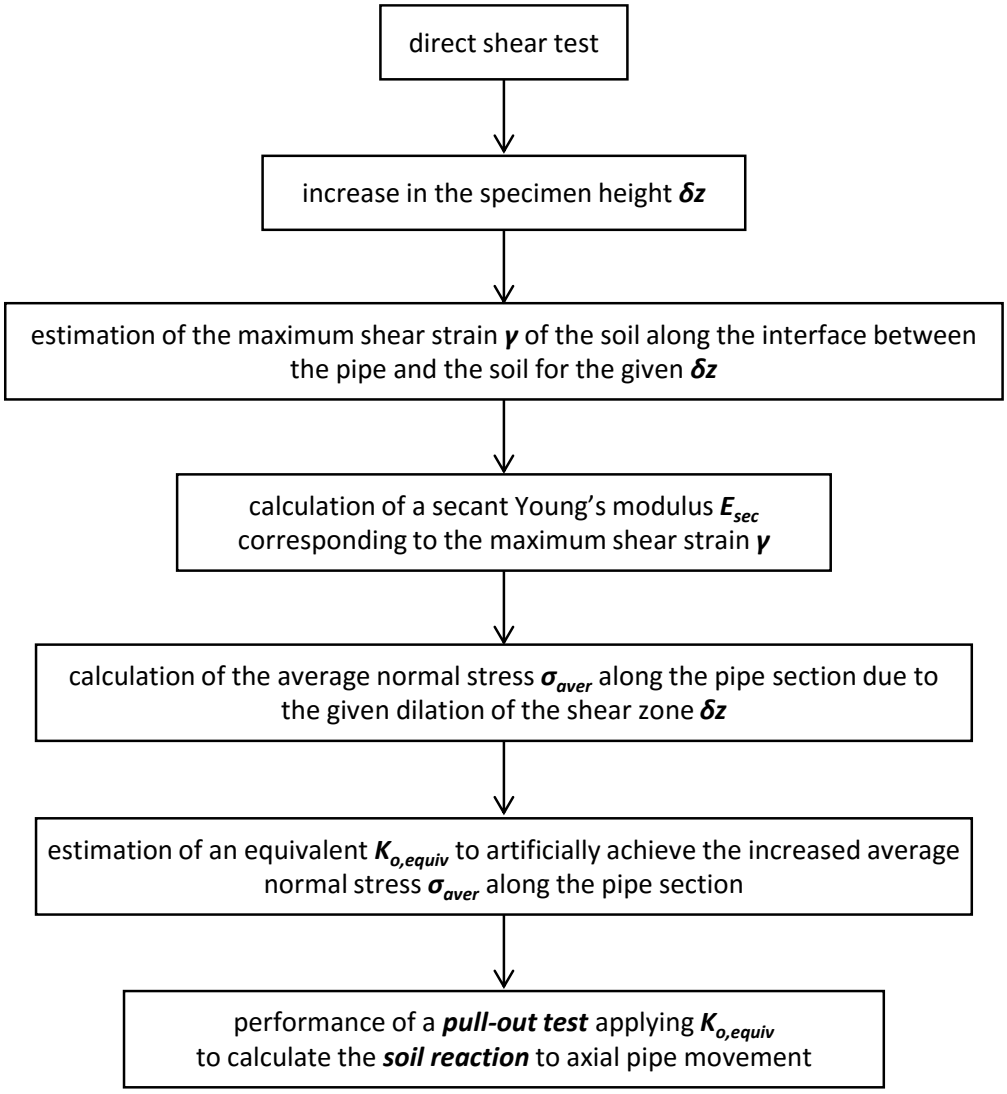

Figure 5. Flowchart presenting the steps of the finite element methodology used to calculate the soil reaction to axial pipe movement.

The proposed Step-by-step FE procedure

Step 1: Estimate the volumetric expansion (δz) of the shear zone by means of direct shear tests. . It is assumed that the increase of the thickness of the shear zone (, if it was not bounded by the outer soil) would have be equal to the vertical displacement δz of a soil specimen subjected to direct shear test. Typical values of shear zone expansion are portrayed in Figure 6 for different values of dilation angle. For example, a pipe embedded in dense sand of $\psi = 25^o$ is expected to experience volumetric expansion δz= 1.2 mm.

Step 2: Estimate the additional normal stresses $\Delta\sigma_n$ caused by the obstruction of the radial expansion of the shear zone.. To this end, an analysis is performed where the pipe diameter is increased by the computed δz (to simulate the tendency of the shear zone to expand), and the average normal stress is measured. Bear in mind that in order to accurately predict this stress, we need to a-priori assume a (secant) shear modulus representative of the magnitude of the developed shear strains – a complication resulting from the assumption of an elastoplastic M-C criterion. Therefore, an elastic analysis of the same problem precedes so as to determine the

maximum shear strain γ that develops in the soil at the immediate vicinity of the pipe section. The secant shear modulus degradation curve proposed by Oztoprak and Bolton (2013) is adopted herein, which correlates maximum shear strain γ and secant shear modulus e. Figure 7 schematically summarizes the required actions for the completion of this step. Figure 7a presents the distribution of shear strain around the pipe, and the evolution of the maximum shear strain with the increase in the pipe diameter. For the example case of $\psi = 25^o$ and δz = 1.2 mm (estimated by Step 1), the maximum experienced shear strain equals γ= 0.48% which corresponds to of G/G_o = 0.063 and to a σ_{aver} = 32.6 kPa (note that average normal stress under geostatic conditions equals $\sigma_{aver,0}$ = 18.6 kPa).

Step 3: Assume an equivalent lateral earth pressure coefficient $K_{o,equiv}$ that yields the target σ_{aver} and calculate the force-displacement behavior of the pipe subjected to pullout test. It is noted that by assuming an increased $K_{o,equiv}$ we are not replicating the actual stress distribution along the pipe periphery, but we manage to correctly capture the increased magnitude of the average normal stress (which eventually is controlling the peak axial load on the pipe Back to our example case, the equivalent lateral earth pressure coefficient is $K_{o,equiv}$ = 1.38. (Figure 8b). Consequently, adopting this $K_{o,equiv}$ we perform a numerical axial pullout test to assess the force-displacement curve. The pipe-soil interface is described by a friction coefficient that depends on the friction angle of the soil ($\mu = \tan(0.8\varphi)$ according to ALA 2001, PRCI 2004 for rough steel). Therefore, at peak conditions it is described by $\mu_{peak} = \tan(0.8x40) = 0.645$ and at residual conditions by $\mu_{res} = \tan(0.8x32) = 0.479$. The deterioration from peak to residual conditions is achieved by an exponential decay of the friction coefficient using a decay constant of k = 25. This constant was selected as a reasonable value following the experience from past studies on the pullout response of pipes available in literature (Scarpelli et al 2003, Wijewickreme et al 2009, GIPIPE final report 2015). Figure 8c presents the axial force-displacement response of the pipe for the various dilation angles considered in this study. Notice that even though in all cases the sand is described by the same shear strength (as dictated by a common $\varphi_{peak} = 40^o$), when the sand exhibits strongly dilative behavior (e.g. $\psi = 25^o$), the maximum soil reaction to axial pipe movement increases by 75% compared to the non-dilative sand (where F_{max} = 56.1 kN/m and F_{max} = 32 kN/m respectively).

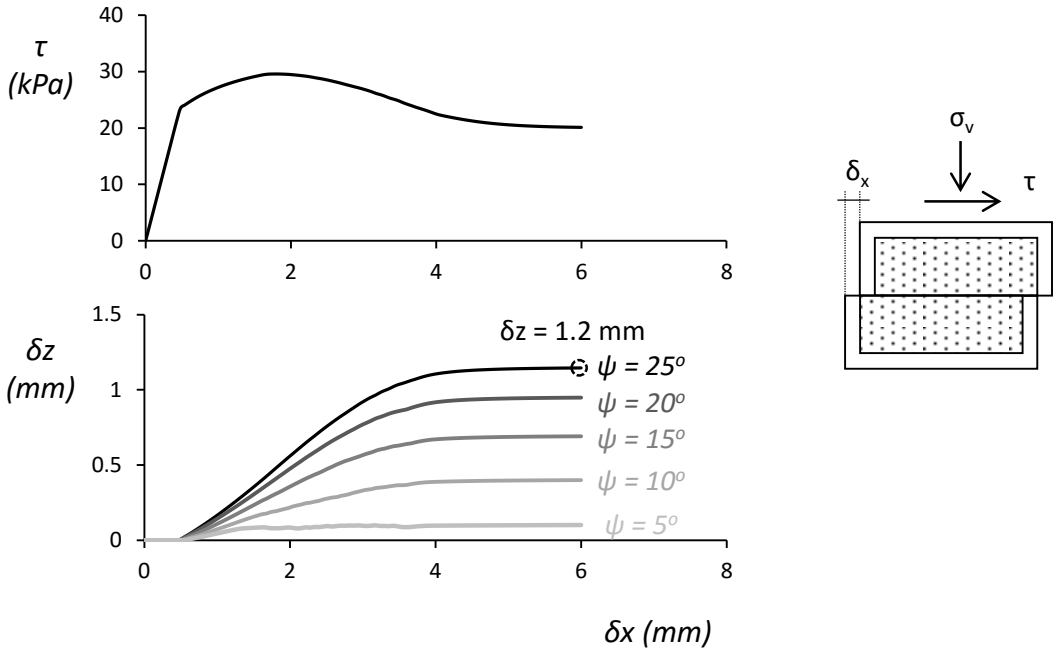

Figure 6. Direct shear testing of a soil element to measure the increase in height δz.

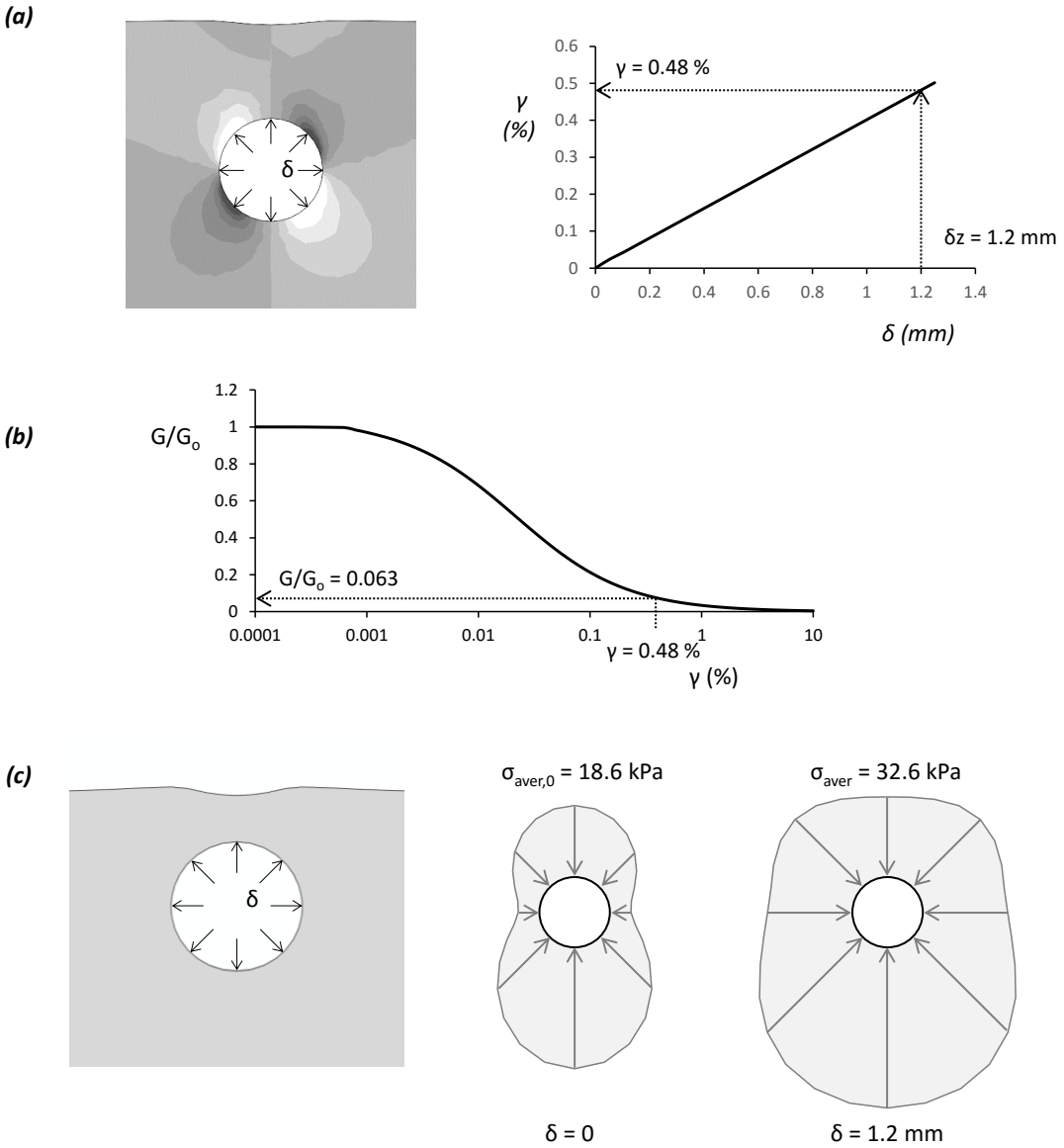

Figure 7. Stress increase along the pipe periphery during axial pullout: (a) Calculation of the maximum shear strain of the soil for the given radial displacement δz. (b) Secant shear modulus (representative of the maximum shear strain developed) (c) calculation of average normal stress σ_{ave} due to pipe diameter expansion by δz

PIPELINE RESPONSE SUBJECTED TO NORMAL FAULT: THE EFFECT OF DILATANCY

Having established a methodology to accurately assess the pull-out capacity of a buried pipeline, we incorporate the latter to the axial springs of the finite element model. In the next set of analyses, the dilation angle of soil ranges between $\psi = 0^o$ and $\psi = 25^o$and the performance of the pipe is parametrically discussed Emphasis is here being placed on the provided margins of safety until the pipeline failure (i.e. rupture of the pipe wall). Following the EN 1998–4 provisions for seismic-fault-induced actions on buried steel pipeline and the seismic provisions of ASCE MOP 119 for buried water steel pipelines, to avoid rupture and possible loss of containment the maximum tensile strain should be lower than a limit value of $\varepsilon_{max} = 3\%$..

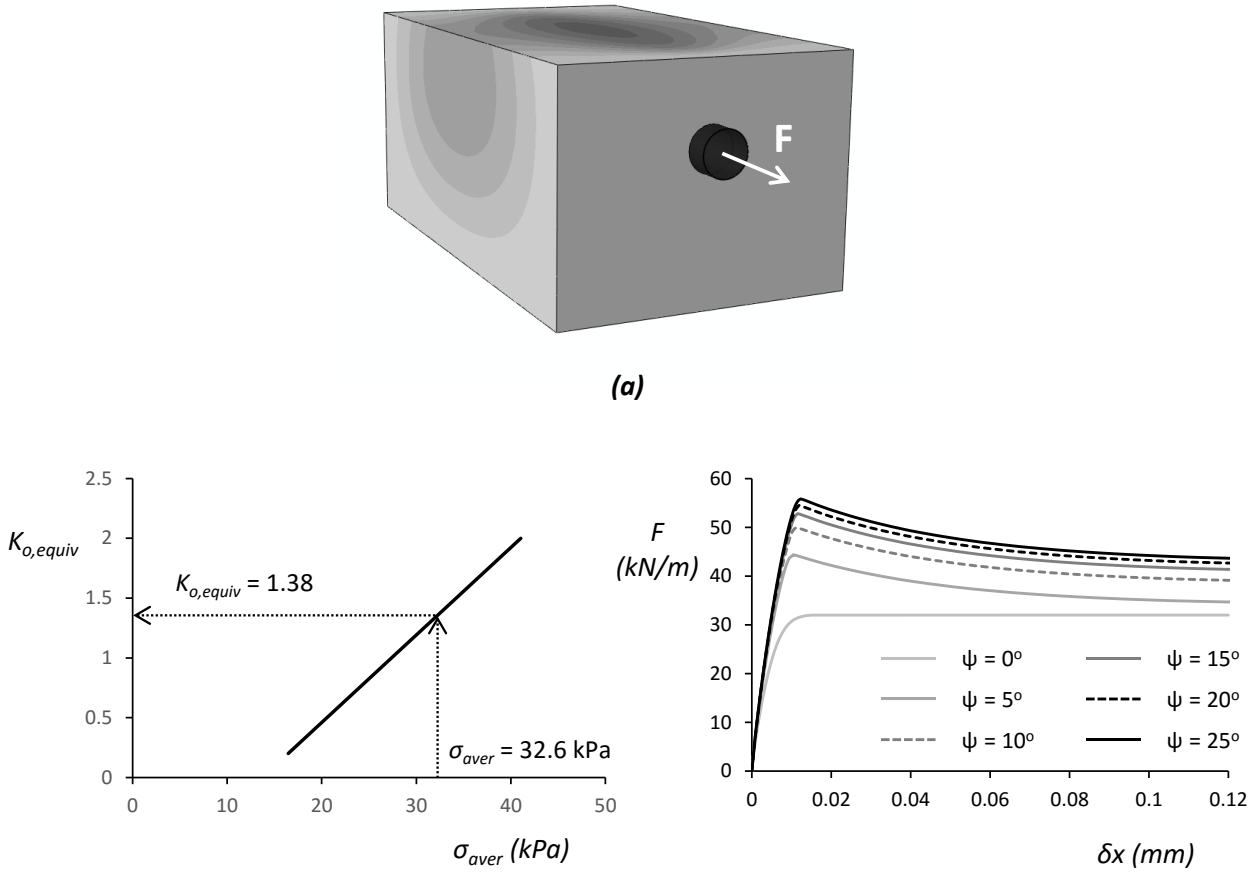

Figure 8. The axial force-displacement response as a function of dilatancy angle: (a) the finite element model employed for the axial pullout test; (b) the equivalent lateral pressure coefficient $K_{o,equiv}$ used to describe the increased average normal stress σ_{aver} around the pipe; (c) the force-displacement curves for varying dilation angles.

Figure 9 displays the response of the example pipeline when embedded in a non-dilative sand (ψ=0). In Figure 9a, the deformed mesh of the model is presented with superimposed displacement contours, focusing on the central 3D region close to the fault. A longitudinal cut has been applied to the model at the location of the pipeline, to make the pipeline deformation visible. As expected, the pipe bends to accommodate the vertical dislocation imposed by the fault, acquiring the characteristic double curvature deformation shape. Two inflection points are formed, one within the hanging wall and another one within the footwall. These are the sections where the maximum curvature is observed and therefore, the maximum bending moment. Among these two points, the one within the footwall develops larger moments since it is stressed further by the reaction of the underlying soil (as opposed to the reaction from the overlying soil which is smaller). On top of this bending stressing, severe tension is also provoked by the imposed increase in length due to the slip deformation along the fault. The combination of these two actions results in large tensile axial strains that accumulate at the top side of the pipe (Figure 9b and Figure 9c). Ultimately, the developed axial strain becomes larger than the strain limit (ε_{max} = 3 %) and the pipeline failure is eminent. Figure 9d portrays the instant of failure by presenting the evolution of the maximum axial strain along the pipeline with the increase in the imposed fault displacement: at δ = 1.14 m the maximum axial strain has abruptly met the failure criterion and the pipe has failed.at

Naturally, the safety margins until failure appear to be significantly affected by the dilative behavior of the sand. This effect is plotted in Figure 10 where the critical fault displacement (that induces pipeline failure) is presented as a function of the dilation angle ψ. Observe that as the dilation angle increases, the soil reaction to axial movement of the pipeline also increases (see Figure 8c). As a result, the tensile stresses due to stretching developed in the central region are growing and ultimately, the safety margins until failure decrease i. For

example a pipe buried in sand of $\psi = 25^o$ will fail at imposed fault displacement δ=0.82 m, while for a non-dilative sand ($\psi = 0^o$) the same pipeline would have sustain an offset of δ = 1.14 m before failure.

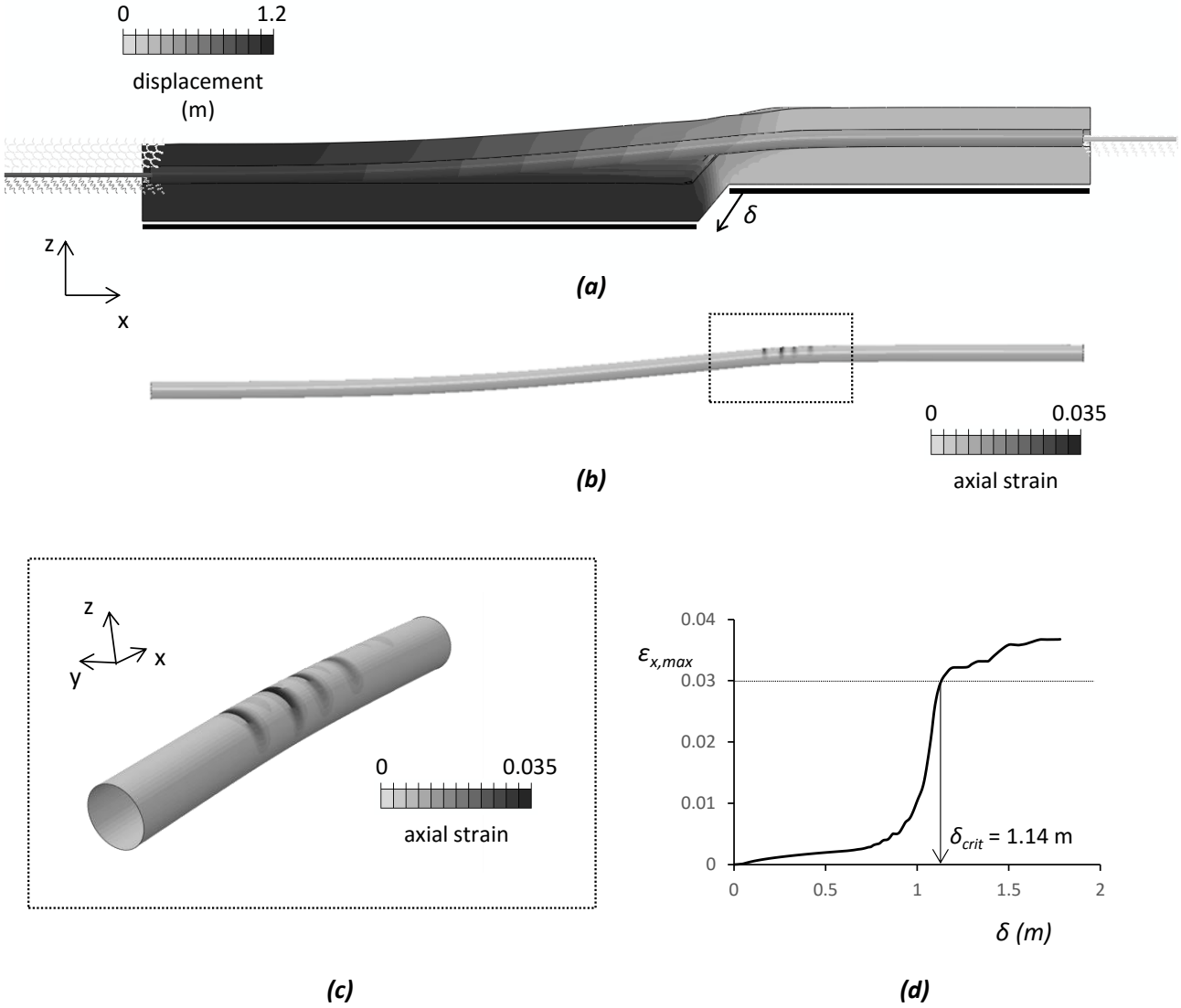

Figure 9. Pipeline buried in non-dilative sand ($\psi = 0^o$) subjected to normal fault: (a) deformed model with superimposed displacement contours; (b) deformed mesh of the pipeline with superimposed axial strain contours. (c) Detail of the pipeline at the critical region. (d) Evolution of the maximum axial strain along the pipeline with increasing fault displacement.

In other words, ignoring the dilative nature of the embedment soil, may lead to a non-conservative design, which is exactly the case with the current code provisions. . Be reminded that in common practice, the maximum soil reaction to axial pipe movement is a function of the initial average normal stress at the pipe-soil interface (as it is approximated by the (1+Ko)/2 expression in Eq2). No recommendation is provided on the effect of dilatancy which evidently may significantly increase the actual resistance.
regardless of the dilation angle of the soil, the existing codes consider the . Failing to account for this type of increase could lead to a significant overestimation of the actual safety margins until failure, and eventually to a risky design. A simplified yet efficient way to account for the effect of dilation is to apply to equation (1) an increased value of lateral earth pressure coefficient $K_{o,equiv}$. The calculation of the appropriate $K_{o,equiv}$ can be performed following the simple finite element methodology presented above.

CONCLUSIONS

This paper numerically investigates the effect of dilative behavior of soil on the response of an infinitely long pipeline subjected to normal faulting. It is recognized in the literature that during the relative pipeline-soil movement in the longitudinal direction, a thin zone around the pipe is actively sheared. Due to this shearing in case of a dilative soil the shear zone tends to increase in volume. Since this displacement is confined, additional stresses are developed at the pipe-soil interface, which in turn increase the soil reaction to the axial pipe movement. This change in the peak value of axial resistance, is controlling the pipeline performance in the event of a normal faulting.

The paper proposed a step –by step procedure to numerically assess the increased axial resistance of highly dilative soils. The procedure is next applied in an example test case of a pipeline (of diameter D = 36 in, thickness t = 12.7 mm, pressure p = 6 MPa) embedded within a dry sand layer of $\varphi = 40^o$ at burial depth H = 1.66, crossing perpendicularly a normal fault with dip angle a = 60^o. By ignoring the effect of dilation (i.e. assuming that ψ=0), the pipe could attain a maximum fault displacement of 1.14 m before reaching failure. Yet, the safety margins decrease drastically if soil dilatancy is explicitly considered (Figure 10) a. Namely, for a dilation angle of $\psi = 25^o$ the maximum offset drops to 0.82 m.

Evidently, the tendency of sands towards dilation should be accounted for in the design of a pipelines subjected to normal fault induced displacements. Even in the case of conventional design (following the API recommendations), an acceptable approach would be to e apply an equivalent lateral earth pressure coefficient $K_{o,equiv}$ (as described previously) rather than the K_o at rest.

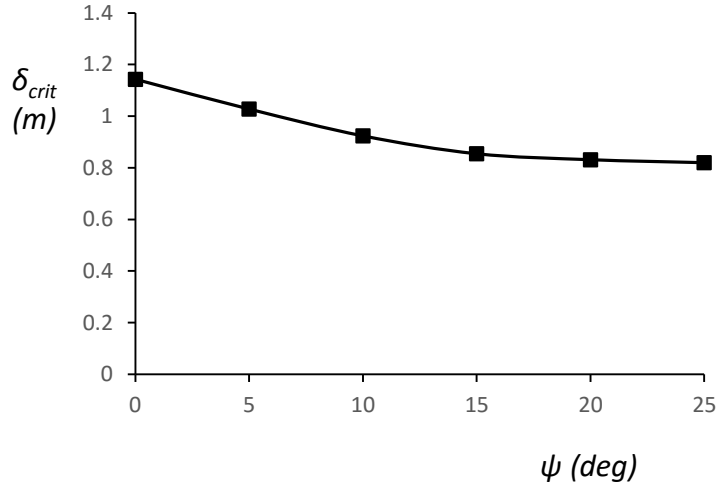

Figure 10. The effect of the soil dilatancy on the pipe performance. The critical fault displacement that leads to failure δ_{crit} with respect to the sand dilatancy ψ.

REFERENCES

American Lifelines Alliance. Guidelines for the design of buried steel pipes, ASCE, New York (2001)

Anastasopoulos, I., Gazetas, G., Bransby, M. F., Davies, M. C. R., & El Nahas, A. (2007). Fault rupture propagation through sand: finite-element analysis and validation through centrifuge experiments. *Journal of Geotechnical and Geoenvironmental Engineering*, *133*(8), 943-958.

Anderson, C., Wijewickreme, D., Ventura, C., & Mitchell, A. (2005). FULL-SCALE LABORATORTY TESTING OF SOIL-PIPE INTERACTION IN BRANCHED POLYETHYLENE PIPELINES. *Experimental Techniques*, *29*(2), 33-a37.

Bridgwater, J. (1980). On the width of failure zones. *Geotechnique*, *30*(4), 533-536.

Cappelletto, A., Tagliaferri, R., Giurlani, G., Andrei, G., Furlani, G., & Scarpelli, G. (1998). Field full scale tests on longitudinal pipeline-soil interaction. In*PROC INT PIPELINE CONF IPC, ASME, FAIRFIELD, NJ,(USA), 1998*, (Vol. 2, pp. 771-778).

Colton, J. D., Chang, P. H. P., & Lindberg, H. E. (1982). Measurement of dynamic soil-pipe axial interaction for full-scale buried pipelines. *International Journal of Soil Dynamics and Earthquake Engineering*, *1*(4), 183-188.

Comite Européen de Normalisation. Eurocode 8, part 4: silos, tanks and pipelines, CEN EN1998-4. Brussels, Belgium; 2006.

DeJong, J. T., White, D. J., & Randolph, M. F. (2006). Microscale observation and modeling of soil-structure interface behavior using particle image velocimetry. *Soils and foundations*, *46*(1), 15-28.

Honegger, D. G. (1999). Field Measurement of Axial Soil Friction Forces on Buried Pipelines. In *Optimizing Post-Earthquake Lifeline System Reliability* (pp. 703-710). ASCE.

Liang, Jianwen, and Shaoping Sun. "Site effects on seismic behavior of pipelines: a review." *Journal of pressure vessel technology* 122.4 (2000): 469-475.

O'Rourke, T. D., & Palmer, M. C. (1996). Earthquake performance of gas transmission pipelines. *Earthquake Spectra*, *12*(3), 493-527.

Oztoprak, S., & Bolton, M. D. (2013). Stiffness of sands through a laboratory test database. *Géotechnique*, *63*(1), 54-70.

Paulin, M. J., Phillips, R., Clark, J. I., Trigg, A., & Konuk, I. (1998). A full-scale investigation into pipeline/soil interaction. In *Conference Preprints*.

PRCI, (2004), "Guidelines for the Seismic Design and Assessment of Natural Gas and Liquid Hydrocarbon Pipelines, Pipeline Design, Construction and Operations", Edited by Honegger, D. G., and Nyman D. J., Technical Committee of Pipeline Research Council International (PRCI) Inc, October 2004.

Roscoe, K. H. (1970). The influence of strains in soil mechanics.*Geotechnique*, *20*(2), 129-170.

Scarpelli, G., Sakellariadi, E., & Furlani, G. (2003). Evaluation of soil–pipeline longitudinal interaction forces. *Rivista Italiana di Geotecnica*, *37*(4), 24-41.

Singhal, A. C. (1980) "Experiments of pipeline joints." American Society of Mechanical Engineers, n 80-C2/PVP-70, 5p.

Tang, A. K. (Ed.). (2000). *Izmit (Kocaeli), Turkey, Earthquake of August 17, 1999 Including Duzce Earthquake of November 12, 1999: Lifeline Performance* (Vol. 17). ASCE Publications.

Uzarski, J., & Arnold, C. (Eds.). (2001). *Chi-Chi, Taiwan, earthquake of September 21, 1999: reconnaissance report* (Vol. 17). Earthquake Engineering Research Institute.

Vardoulakis, I., & Graf, B. (1985). Calibration of constitutive models for granular materials using data from biaxial experiments. *Geotechnique*, *35*(3), 299-317.

Whidden, W. R. (2009). *Buried flexible steel pipe: design and structural analysis*. American Society of Civil Engineers (ASCE).

Wijewickreme, D., Karimian, H., & Honegger, D. (2009). Response of buried steel pipelines subjected to relative axial soil movement. *Canadian Geotechnical Journal*, *46*(7), 735-752.

European Commission, Directorate-General for Research and Innovation (2015), "*Safety of buried steel pipelines under ground-induced deformations (GIPIPE)*", ISBN: 978-92-79-54040-0